Origin of diffraction fringes in two-dimensional photoelectron momentum distributions for single ionization of atoms in few-cycle intense laser pulses*

Guo Zhi-Jian(郭志坚)[a], Chen Zhang-Jin(陈长进)[b]†, and Zhou Xiao-Xin(周效信)[a]

[a] College of Physics and Electronic Engineering, Northwest Normal University, Lanzhou 730070, China

[b] Department of Physics, College of Science, Shantou University, Shantou 515063, China

(Received 17 August 2013; revised manuscript received 14 September 2013; published online 10 February 2014)

We use the strong field approximation with a time window function controlling the release time of electrons to study the intra-cycle and inter-cycle interferences in few-cycle intense laser pulses impinging on He. The diffraction fringes, i.e., the vertical stripe-like structure, observed in the experimental two-dimensional photoelectron momentum distributions of Gopal *et al.* (2009 *Phys. Rev. Lett.* **103** 053001) have been attributed to the interplay of the intra- and inter-cycle interferences. The pure numerical calculations by solving the time-dependent Schrödinger equation are also performed and the results are compared with the experimental measurements directly. It has been found that the position of the stripe-like structure can be used to determine the duration of the laser pulses used in experiments.

Keywords: intra-cycle and inter-cycle interferences, stripe-like structure, two-dimensional momentum distributions

PACS: 32.80.Rm, 32.80.Fb **DOI:** 10.1088/1674-1056/23/4/043201

1. Introduction

Single ionization of rare gas atoms in intense laser pulses has been extensively studied and most of the phenomena have been well understood. The ionization takes place through either a multiphoton or a tunneling mechanism depending on the value of the Keldysh parameter $\gamma = \sqrt{I_p/2U_p}$, where I_p is the ionization energy and U_p is the ponderomotive potential. It has been well recognized that in a multiphoton ionization process, in which $\gamma > 1$, an electron absorbs more photons than necessary and the resulting photoelectron energy spectra show characteristic ATI (above-threshold ionization) peaks separated by the photo-energy with the positions shifted by the ponderomotive potential. On the other hand, as the laser intensity increases such that $\gamma < 1$, the valence electron tunnels through the potential barrier formed by the combination of the atomic potential and the external strong field.

While the photoelectron energy spectra carry the basic information about the ionization processes, more detailed information can be obtained by the study of the two-dimensional momentum distributions (2DMD). To our knowledge, the first measurements on fully 2DMD with high-resolution for single ionization of atoms by short intense laser pulses were carried out by Rudenko *et al.*[1] in 2004, and similar measurements were performed by Maharjan *et al.*[2] two years later. Besides the typical ATI pattern, the experimental measurements on the 2DMD also show energy features that do not move with laser intensity, indicating possible multi-photon resonances,[3] and the radial fan-like structures attributed to Coulomb-focusing.[4]

With the fast development of laser techniques, the generation of few-cycle optical pulses with durations of less than 10 fs corresponding to fewer than four cycles has become routine in several laser laboratories. Ultrashort pulses with durations comparable to the optical period associated with the carrier frequency lead to novel features of laser–matter interactions, among which the most remarkable one is the strong carrier-envelope phase (CEP) dependence of excitation and ionization processes.[5–8] The major technological advance in recent years in ultrafast lasers is the stabilization of the CEP. Although it turns out that it is extremely difficult to stabilize the CEP, especially to high precision, the recent development in Ref. [9] allows experimentalists to measure electron spectra and monitor the shot-to-shot CEP variation. With CEP stabilized few-cycle intense laser pulses, the features in the photoelectron 2DMD are markedly different from the typical ATI spectra for longer pulses with well-defined ponderomotive energy.

Since the pioneering attosecond double-slit experiment in the time domain by Lindner *et al.*,[10] the intra-cycle and inter-cycle interferences have recently attracted considerable interest both experimentally[11] and theoretically.[12–16] In the tunneling ionization regime, electron emission occurs within each optical cycle predominantly around the maxima of the absolute value of the electric field. For a few-cycle intense laser

*Project supported by the National Natural Science Foundation of China (Grant Nos. 11274219 and 11264036), the STU Scientific Research Foundation for Talents, and the Scientific Research Foundation for the Returned Overseas Chinese Scholars, State Education Ministry, China.

†Corresponding author. E-mail: chenzj@stu.edu.cn

© 2014 Chinese Physical Society and IOP Publishing Ltd

pulses, the emission is temporally confined to a few adjacent field maxima. It is the interference of the successive bursts of ejected electrons reaching the same final momentum in ultrashort pulses that accounts for the "unusual" features which are not found in the ATI spectra in multicycle pulses.

Recently certain unusual features have been observed in the experiment by Gopal *et al.*[11] for single ionization of helium by 5-fs CEP stabilized laser pulses with a carrier wavelength of 740 nm at a peak intensity of 4×10^{14} W/cm^2. In the measured 2DMD, clear stripe-like fringes were observed for CEPs with maximum asymmetry.

The goal of this work is to understand and analyze the experimental measurements in Ref. [11]. By using a model based on strong field approximation (SFA),[17] we demonstrate how the stripe-like fringes are formed. We also present results from an *ab initio* solution of the time-dependent Schrödinger equation (TDSE). Atomic units $m_e=\hbar=e=1$ are used throughout the paper unless otherwise indicated.

2. Theory

We consider the interaction of atoms with linearly polarized laser pulses with the electric field along the z axis,

$$\boldsymbol{E}(t)=E_0a(t)\cos(\omega t+\phi)\hat{z}, \tag{1}$$

where ω is the frequency of the carrier wave and ϕ is the CEP with the envelope function $a(t)$ chosen to be

$$a(t)=\cos^2\left(\frac{\pi t}{T}\right) \tag{2}$$

for the time interval $(-T/2,\ T/2)$ and zero elsewhere. The pulse duration Γ, defined as the full-width at half-maximum (FWHM), is then related to T by $\Gamma=T/2.75$.

In this section, we briefly summarize the SFA and TDSE which are used to simulate the 2DMD for the ionization of atoms exposed in strong laser fields. The details of the SFA and the numerical method for solving the TDSE have been presented by Chen *et al.*[4,18]

2.1. The SFA

In the SFA model, the momentum-dependent ionization amplitude, including only the first two terms of the perturbation series, is given by

$$f(\boldsymbol{p})=f_1(\boldsymbol{p})+f_2(\boldsymbol{p}), \tag{3}$$

where $\boldsymbol{p}$ is the momentum of the detected photoelectron.

In Eq. (3), the first term $f_1(\boldsymbol{p})$, which is actually the traditional SFA, will be referred to as SFA1. The SFA1 is given by

$$f_1(\boldsymbol{p})=-\mathrm{i}\int_{-\infty}^{\infty}\mathrm{d}t\,\langle\chi_{\boldsymbol{p}}(t)\,|H_i(t)|\,\Psi_i(t)\rangle\,, \tag{4}$$

where $H_i(t)$ is the atom–field interaction in the form

$$H_i(t)=\boldsymbol{r}\cdot\boldsymbol{E}(t), \tag{5}$$

and Ψ_i is the ground state wave function, which can be expressed by

$$\Psi_i(t)=R_{n_il_i}(r)Y_{l_im_i}(\hat{\boldsymbol{r}})\,\mathrm{e}^{-\mathrm{i}E_it}, \tag{6}$$

where E_i and $R_{n_il_i}$ are the energy and the radial wave function of the ground state, respectively. By introducing the new radial function

$$u_{n_il_i}=rR_{n_il_i}, \tag{7}$$

the radial wave function is obtained numerically by solving the differential equation

$$\left[-\frac{1}{2}\frac{\mathrm{d}^2}{\mathrm{d}r^2}+V_{\mathrm{eff}}(r)\right]u_{n_il_i}=E_iu_{n_il_i}, \tag{8}$$

where $V_{\mathrm{eff}}(r)$ is the effective potential related to the atomic central potential $V(r)$ by

$$V_{\mathrm{eff}}(r)=\frac{l(l+1)}{2r^2}+V(r). \tag{9}$$

In the single-active-electron approximation, the model potential for atoms is parametrized in the form

$$V(r)=-\frac{1+a_1\,\mathrm{e}^{-a_2r}+a_3r\,\mathrm{e}^{-a_4r}+a_5\,\mathrm{e}^{-a_6r}}{r}. \tag{10}$$

The parameters in Eq. (10) are obtained by fitting the calculated binding energies from this potential to the experimental binding energies of the ground state and the first few excited states of the target atom.[19]

The Volkov state $\chi_{\boldsymbol{p}}$ in Eq. (4) is given by

$$\langle\boldsymbol{r}|\chi_{\boldsymbol{p}}(t)\rangle=\frac{1}{(2\pi)^{3/2}}\,\mathrm{e}^{\mathrm{i}[\boldsymbol{p}+\boldsymbol{A}(t)]\cdot\boldsymbol{r}}\,\mathrm{e}^{-\mathrm{i}S(\boldsymbol{p},t)}, \tag{11}$$

where the action S is

$$S(\boldsymbol{p},t)=\frac{1}{2}\int_{-\infty}^{t}\mathrm{d}t'\left[\boldsymbol{p}+\boldsymbol{A}(t')\right]^2. \tag{12}$$

To evaluate the SFA1 amplitude, we rewrite Eq. (4) as

$$\begin{aligned}f_1(\boldsymbol{p})\ =\ &-\mathrm{i}\frac{1}{(2\pi)^{3/2}}\int_{-\infty}^{\infty}\mathrm{d}tE(t)\,\mathrm{e}^{\mathrm{i}S(\boldsymbol{p},t)}\,\mathrm{e}^{\mathrm{i}I_{\mathrm{p}}t}\\&\times\int\mathrm{d}\boldsymbol{r}\,\mathrm{e}^{-\mathrm{i}[\boldsymbol{p}+\boldsymbol{A}(t)]\cdot\boldsymbol{r}}z\Psi_i(\boldsymbol{r}),\end{aligned} \tag{13}$$

where $I_{\mathrm{p}}=-E_i$ is the ionization potential of the ground state. To perform integration over space coordinates in Eq. (13), we use the identity

$$\mathrm{e}^{-\mathrm{i}\boldsymbol{q}\cdot\boldsymbol{r}}=4\pi\sum_{lm}\mathrm{i}^{-l}\mathrm{j}_l(qr)Y_{lm}(\hat{\boldsymbol{r}})Y^*_{lm}(\hat{\boldsymbol{q}}), \tag{14}$$

where $\mathrm{j}_l(qr)$ is the spherical Bessel function. By using $z=\sqrt{4\pi/3}rY_{10}(\hat{\boldsymbol{r}})$, the integral over space coordinates can be expressed

$$\Psi_0(\boldsymbol{q})\ \equiv\ \int\mathrm{d}\boldsymbol{r}\,\mathrm{e}^{-\mathrm{i}\boldsymbol{q}\cdot\boldsymbol{r}}z\Psi_i(\boldsymbol{r})$$

$$= 4\pi\sqrt{\frac{4\pi}{3}}\sum_{lm} \mathrm{i}^{-l} Y_{lm}(\hat{\boldsymbol{q}}) \int \mathrm{d}r r^3 R_{n_i l_i}(r) \mathrm{j}_l(qr) \times \int \mathrm{d}\hat{\boldsymbol{r}} Y^*_{lm}(\hat{\boldsymbol{r}}) Y_{10}(\hat{\boldsymbol{r}}) Y_{l_i m_i}(\hat{\boldsymbol{r}}). \quad (15)$$

Note that although we focus in this work on helium, the above expressions are universal. In the numerical calculations, only $m_i = 0$ is taken into account in Eq. (15) even for $l_i = 1$ for Ar, for example, since it is well known that for linearly polarized laser pulses, the contribution to the ionization probability from $m_i = \pm 1$ is relatively much smaller in comparison to the $m_i = 0$ component. Consequently, the integral over a solid angle is given by

$$\int \mathrm{d}\hat{\boldsymbol{r}} Y^*_{lm}(\hat{\boldsymbol{r}}) Y_{10}(\hat{\boldsymbol{r}}) Y_{l_i m_i}(\hat{\boldsymbol{r}}) = \sqrt{\frac{3(2l_i+1)}{4\pi(2l+1)}} C(1 l_i l; 000) C(1 l_i l; m_i 0 m_i) \delta_{m m_i}, \quad (16)$$

where the C's are the Clebsch–Gordan coefficients.

While the SFA1 accounts for direct ionization, the second term $f_2(\boldsymbol{p})$ in Eq. (3), which will be called SFA2, describes rescattering of laser-induced electrons with the parent ion. The SFA2 term is expressed as

$$f_2(\boldsymbol{p}) = -\int_{-\infty}^{\infty} \mathrm{d}t \int_t^{\infty} \mathrm{d}t' \int \mathrm{d}\boldsymbol{k} \langle \chi_{\boldsymbol{p}}(t') | V | \chi_{\boldsymbol{k}}(t') \rangle \times \langle \chi_{\boldsymbol{k}}(t) | H_i(t) | \Psi_i(t) \rangle . \quad (17)$$

The details of the numerical procedure for evaluating SFA2 can be found in Refs. [17] and [18].

With the momentum-dependent ionization amplitude, the angular and momentum distribution of the emission of an electron with energy $E = p^2/2$ in the direction of $\hat{\boldsymbol{p}}$ is given by

$$\frac{\mathrm{d}^3 P}{\mathrm{d}^3 \boldsymbol{p}} = |f(\boldsymbol{p})|^2. \quad (18)$$

For a linearly polarized laser field, the system has cylindrical symmetry. As a result, we can define the 2DMD as

$$\frac{\mathrm{d}^2 P}{\mathrm{d}p_\perp \mathrm{d}p_z} = |f(\boldsymbol{p})|^2 2\pi p \sin\theta, \quad (19)$$

where $p_\perp = \sqrt{p_x^2 + p_y^2}$ and θ is the angle between the polarization axis of the laser field and the direction of the ejected photoelectron. Obviously, the integration over the azimuthal angle φ has been carried out in Eq. (19). Furthermore, by integrating over θ, we get the energy spectra

$$\frac{\mathrm{d}P}{\mathrm{d}E} = 2\pi\sqrt{2E} \int_{-1}^{+1} |f(\boldsymbol{p})|^2 \mathrm{d}(\cos\theta). \quad (20)$$

2.2. The TDSE

While the SFA is of great interest for analyzing features of the intense laser–atom interaction, the direct solution of the Schrödinger equation in a time-dependent laser field provides an accurate reliable full quantum description of the ATI spectra which can be used to evaluate the validity of all types of approximations. Within the single-active-electron approximation, the TDSE for an atom in the presence of a linearly polarized laser field, in the length gauge, can be written as

$$\mathrm{i}\frac{\partial}{\partial t}\Psi(\boldsymbol{r},t) = \left[-\frac{1}{2}\nabla^2 + V(r) + H_i(t)\right]\Psi(\boldsymbol{r},t). \quad (21)$$

The time-dependent equation is solved by using a second-order split operator method,[20,21] and the wave function is expanded by the direct products of discrete variable representation basis sets[22–24] associated with Legendre polynomials.

The photoelectron yield is obtained by projecting the total final wave function at the end of the laser pulse onto eigenstates of a continuum electron with momentum $\boldsymbol{p}$,

$$\frac{\mathrm{d}^3 P}{\mathrm{d}^3 \boldsymbol{p}} = \left| \langle \Phi_{\boldsymbol{p}}^- | \Psi(t = T/2) \rangle \right|^2, \quad (22)$$

where the continuum state $\Phi_{\boldsymbol{p}}^-$ is the outgoing asymptotic Coulomb wave function satisfying the following equation

$$\left[-\frac{1}{2}\nabla^2 + V(r)\right]\Phi_{\boldsymbol{p}}^- = \frac{p^2}{2}\Phi_{\boldsymbol{p}}^-. \quad (23)$$

3. Result and discussion

3.1. The SFA simulations

We use the SFA to simulate the experimental measurements in Ref. [11]. To investigate the intra-cycle and inter-cycle interferences, we introduce a time window function $W(t_i)$ to control the electron emission time, such that the electric field is replaced by

$$\tilde{E}(t) = E(t)\sum_{i=1}^{n} W(t_i), \quad (24)$$

where the window function is defined as

$$W(t_i) = \begin{cases} 1, & |t - t_i| < \Delta t/2, \\ 0, & |t - t_i| \geq \Delta t/2, \end{cases} \quad (25)$$

with Δt being the time interval from which the electron is released. Here we choose Δt=0.01τ, where τ is the period of the electric field.

The electric field and the vector potential of a laser pulse of 5 fs at 740 nm with the CEP of $\phi = 0$ and $\phi = \pi/2$ are plotted in Fig. 1, in which the centers of the time windows are marked.

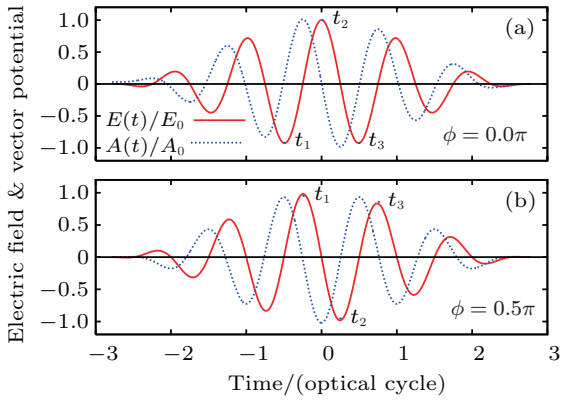


Fig. 1. (color online) The electric field and the vector potential of a laser pulse of 5 fs at 740 nm with the CEP of (a) $\phi = 0$ and (b) $\phi = \pi/2$. The marked times t_i ($i = 1$, 2, and 3) are the centers of the time windows with a width of 0.01 times of the optical cycle for the detached time of the electron.

The 2DMD for single ionization of He in a laser pulse shown in Fig. 1(a) with restricted release times (t_1, t_2), (t_1, t_3), and (t_1, t_2, t_3) are displayed in Fig. 2. To understand the interference patterns in the momentum spectra, we rewrite the SFA1 amplitude in Eq. (13), by replacing the time integration by a discrete sum over the number of release times, as

$$\tilde{f}_1(\boldsymbol{p}) = -\mathrm{i}\frac{1}{(2\pi)^{3/2}}\int_{-\infty}^{\infty} \mathrm{d}t \Psi_0(\boldsymbol{q})\tilde{E}(t)\,\mathrm{e}^{\mathrm{i}S(\boldsymbol{p},t)}\,\mathrm{e}^{\mathrm{i}I_\mathrm{p}t} \sim \sum_{i=1}^{n} \Psi_0(\boldsymbol{q}_i)E(t_i)\,\mathrm{e}^{\mathrm{i}S(\boldsymbol{p},t_i)}\,\mathrm{e}^{\mathrm{i}I_\mathrm{p}t_i}, \tag{26}$$

where $\boldsymbol{q}_i = \boldsymbol{p} + \boldsymbol{A}(t_i)$. Furthermore, for simplicity, we ignore the envelope change between t_1, t_2, and t_3 such that $|E(t_i)| = E_0$ and $|A(t_i)| = 0$ ($i = 1, 2$, and 3). Consequently, the full-space momentum distribution for the interference between two release times t_b and t_a is given by

$$\frac{\mathrm{d}^3\tilde{P}}{\mathrm{d}^3\boldsymbol{p}} \propto |\Psi_0(\boldsymbol{p})|^2[1+\cos(\Delta S + I_\mathrm{p}\Delta t)], \tag{27}$$

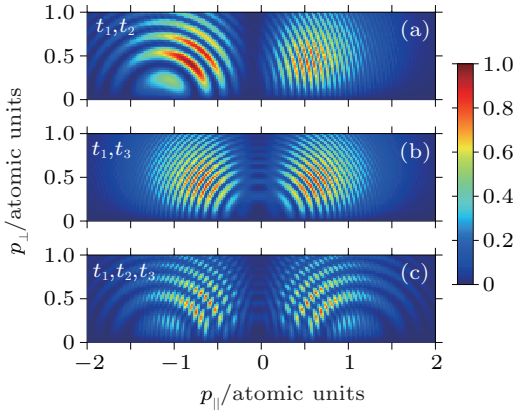


Fig. 2. (color online) The SFA1 two-dimensional momentum distributions for single ionization of helium by a 5-fs pulse with a wavelength of 740 nm at an intensity of 4.0×10^{14} W/cm^2 with a CEP of $\phi = 0$ as shown in Fig. 1(a). (a) Intra-cycle interference between t_1 and t_2. (b) Inter-cycle interference between t_1 and t_3. (c) Total interference (intra- and inter-cycle interferences) between t_1, t_2, and t_3.

where $\Delta t = t_b - t_a$, and

$$\Delta S = \frac{1}{2}\int_{t_a}^{t_b} \mathrm{d}t' \left[\boldsymbol{p} + \boldsymbol{A}(t')\right]^2. \tag{28}$$

From Eq. (27) one can see that the interference pattern in the photoelectron momentum distributions is mainly determined by the difference of action between two times from which the electron wave packets are launched.

For a flat envelop pulse, the difference in the quasi-classical action between any two release times marked in Fig. 1 becomes

$$\Delta S = \frac{1}{2}\left\{p^2\Delta t + \frac{A_0^2}{2}\Delta t + \frac{\tau}{\pi}\frac{A_0}{E_0}p_{||}\left[E(t_b) - E(t_a)\right]\right\}. \tag{29}$$

From Eq. (27), it is easy to see that the maxima in the momentum distributions satisfy the following condition

$$\cos(\Delta S + I_\mathrm{p}\Delta t) = 1, \tag{30}$$

from which one obtains

$$p_\perp^2 + p_{||}^2 + \frac{\tau A_0}{\pi \Delta t E_0}p_{||}\left[E(t_b) - E(t_a)\right] = \frac{4n\pi}{\Delta t} - 2I_\mathrm{p} - 2U_\mathrm{p}. \tag{31}$$

For the case in Fig. 2(a), where $t_b = t_2 = 0$, and $t_a = t_1 = -\tau/2$, the interference criterium in Eq. (30) is given by

$$p_\perp^2 + \left(p_{||} + \frac{2A_0}{\pi}\right)^2 = 2(2n\omega - I_\mathrm{p} - U_\mathrm{p}) + \left(\frac{2A_0}{\pi}\right)^2. \tag{32}$$

Equation (32) clearly demonstrates that the intra-cycle inference generates the 2DMD which are the circles centered at $p_\perp = 0$ and $p_z = -2A_0/\pi$, and each of the circles is separated by 2 times of the photon energy. This is exactly what the numerical simulations reproduced, as shown in Fig. 2(a).

On the other hand, for the case in Fig. 2(b), where $t_b = t_3 = \tau/2$, and $t_a = t_1 = -\tau/2$, the interference criterium becomes

$$p_\perp^2 + p_{||}^2 = 2(n\omega - I_\mathrm{p} - U_\mathrm{p}). \tag{33}$$

It is not surprising at all to see that Eq. (33) predicts nothing but the ATI rings centered at the origin, as shown in Fig. 2(b).

When three consecutive release times are involved, as shown in Fig. 2(c), both the intra- and inter-cycle interference patterns are imprinted in the 2DMD. It can be seen from Fig. 2(c) that the 2DMD are superpositions of the center-shifted circles due to intra-cycle interference and the ATI rings due to inter-cycle interference. As a result, vertical stripes are generated nearby the $p_{||}$ axis for $p_\perp \simeq 0.25$, which were observed in the recent experimental measurements by Gopal *et al.*[11]

It should be noted that the intra-cycle and inter-cycle interferences have been analyzed by Arbó *et al.*[16] by means of saddle point approximation and by Remetter *et al.*[25] using

a sequence of extreme-ultraviolet attosecond pulses combined with an infrared laser field, in which a similar interference criterium was derived, but in a different way.

In Fig. 3, we show the energy spectra calculated by using SFA1 for single ionization of helium corresponding to the 2DMD in Fig. 2. One can see from Fig. 3(a) that for the intra-cycle interference, small oscillations appear in the energy spectra with expanding separation and decreasing strength as the electron energy increases. For the inter-cycle interference between t_1 and t_3, strong regular ATI peaks prevail in the energy spectra as expected, as shown in Fig. 3(b). Furthermore, when both intra- and inter-cycle interferences are involved, the ATI peaks survive, as can be seen from Fig. 3(c).

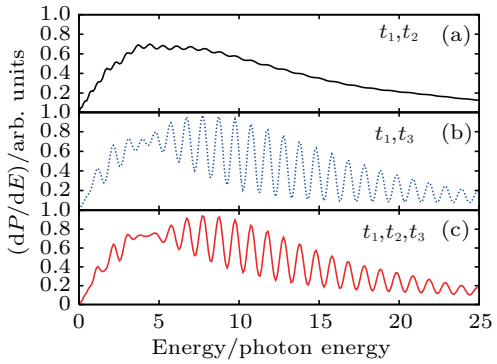


Fig. 3. (color online) The SFA1 energy spectra for single ionization of helium by a 5-fs pulse with a wavelength of 740 nm at an intensity of 4.0×10^{14} W/cm^2 with a CEP of $\phi=0$ as shown in Fig. 1(a). (a) Intra-cycle interference between t_1 and t_2. (b) Inter-cycle interference between t_1 and t_3. (c) Total interference (intra- and inter-cycle interference) between t_1, t_2, and t_3.

For the few-cycle short pulses considered here, the photoelectron spectra are CEP-dependent. To illustrate the CEP dependence, in Fig. 4, we show the same 2DMD as those in Fig. 2 but for laser pulse with the CEP of $\phi=\pi/2$, as shown in Fig. 1(b). While the main feature remains the same, a few discrepancies exist. In Fig. 4(a), the interference center shifts to the right side due to the fact that the change of electric field $E(t_2)-E(t_1)<0$ (see Fig. 1(b)) while for the case in Fig. 2(a), $E(t_2)-E(t_1)>0$. In addition, due to the envelope, the center of the ATI rings in Fig. 4(b) slightly moves away from the origin because $E(t_3)-E(t_1)\neq0$, and the spectra in Fig. 4(c) are not symmetric about $p_{||}=0$.

Once the origin of the vertical stripe-like structure in the 2DMD has been tracked, we perform the numerical simulations using the SFA model for the single ionization of helium in full laser pulses. First, we choose the same laser parameters as those used in the experiment[11] and display the results in Fig. 5(a). Compared with the wide spread of distributions with two centers at $(p_{||}\simeq\pm2A_0/\pi, p_\perp=0)$ in Fig. 4(c), the momentum spectra shrink to a lower energy region where much more enhanced vertical stripes are generated. In addition, the maximum asymmetry in the 2DMD is obtained at the CEP of $\phi=\pi/2$. As a result, the characteristic interference patterns, i.e., the three strong vertical stripes observed in the experimental measurements on the right side in the region of $0.38<p_{||}<0.62$ (see Fig. 4 in Ref. [11]) are very well reproduced.

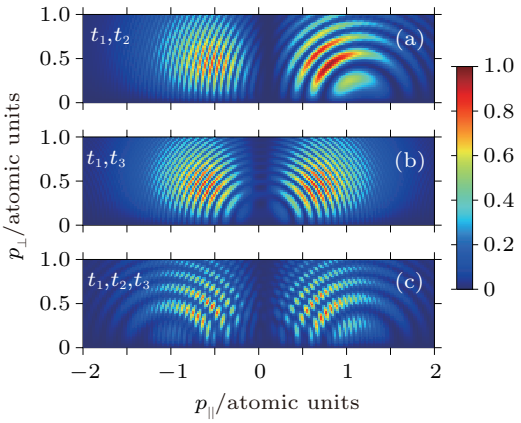


Fig. 4. (color online) The SFA1 two-dimensional momentum distributions for single ionization of helium by a 5-fs pulse with a wavelength of 740 nm at an intensity of 4.0×10^{14} W/cm^2 with a CEP of $\phi=\pi/2$, as shown in Fig. 1(b). (a) Intra-cycle interference between t_1 and t_2. (b) Inter-cycle interference between t_1 and t_3. (c) Total interference (intra- and inter-cycle interference) between t_1, t_2, and t_3.

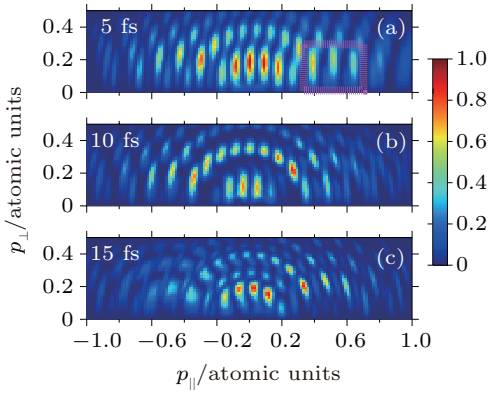


Fig. 5. (color online) The SFA1 two-dimensional momentum distributions for single ionization of helium by (a) 5-fs, (b) 10-fs, and (c) 15-fs laser pulses with a wavelength of 740 nm at an intensity of 4.0×10^{14} W/cm^2 with a CEP of $\phi=\pi/2$. In panel (a), the three strong vertical stripes observed in the experimental measurements on the right side in the region of $0.38<p_{||}<0.62$ are marked by a rectangle.

The vertical stripe-like interference pattern gradually disappears as the pulse duration increases, as illustrated in Figs. 5(b) and 5(c) for pulse durations of 10 fs and 15 fs, respectively. This might indicate that in multicycle pulses, the inter-cycle interference dominates while the intra-cycle interference is suppressed. It should be noted that the vertical stripes in the low energy region corresponding to the first ATI peak in Fig. 5(b) are not due to the intra-cycle interference. This low energy structure in the 2DMD has been investigated by Chen *et al.*[4] in which it is demonstrated that the neglect of the long range Coulomb potential in the SFA model accounts for this structure.

It should be emphasized that we have also performed the SFA2 calculations (the results are not shown in this paper) and confirmed that the SFA2 contributions do not make any visible change to the spectra shown in this paper. It has been well established that the SFA2 accounts for the high-energy "plateau" photoelectrons above $4U_p$.[18] Although in the energy region from $2U_p$ to $4U_p$ the SFA2 is comparable to the SFA1, for the energies less than $2U_p$, the SFA1 absolutely dominates.

3.2. The TDSE results

We also calculate the electron-momentum spectra by solving the TDSE of a one-electron model atom in the laser field. Since it is much more time consuming to solve the TDSE than the SFA and the stripe-like structure does not appear in long pulses according to the SFA results shown in Fig. 5, only the TDSE calculations for laser pulses shorter than 5 fs have been performed. In Fig. 6, we show the 2DMD from TDSE for single ionization of helium by laser fields with pulse durations of $\Gamma = 5$ fs, 4 fs, and 3 fs. One can see that the stripe-like structure can also be predicted by TDSE as long as the pulse duration is less than 5 fs. However, while the stripe-like structure is reproduced with 5-fs and 4-fs pulses at the same region of $p_{||} > 0.3$ as that observed in experiment, as shown in Figs. 6(a) and 6(b), it shifts to lower momenta along the $p_{||}$ axis if shorter pulses are used, as can be seen in Fig. 6(c). In addition, different from the 2DMD from SFA in Fig. 5(a), the ring of the first ATI peak shows the fan-like radial structure in Fig. 6(a). This is a general feature of the two-dimensional electron momentum distributions from the full TDSE solutions.[4] Even for shorter pulses with $\Gamma = 4$ fs and 3 fs, as shown in Figs. 6(b) and 6(c), the fan-like radial structure remains for the low energy region. This indicates that the long-range Coulomb interaction between the outgoing photoelectron and the residual core plays a very important role in low energy spectra.

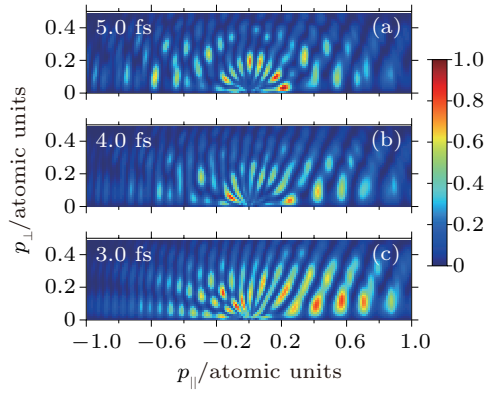


Fig. 6. (color online) The TDSE two-dimensional momentum distributions for single ionization of helium by (a) 5-fs, (b) 4-fs, and (c) 3-fs laser pulses with a wavelength of 740 nm at an intensity of 4.0×10^{14} W/cm^2 with a CEP of $\phi = \pi/2$.

To compare with the experiment, the focal-volume effect[21] has to be taken into account. According to the above analyses, the length of the laser pulses used in the experiment is between 4 fs to 5 fs. Therefore, we compare the volume-integrated TDSE results for $\Gamma = 5$ fs and 4.5 fs with the experimental measurements directly in Fig. 7. Unfortunately, the digital data of the experimental measurements are not available so that the experimental 2DMD cannot be plotted in the same color coordinate as the theoretical results. Nevertheless, one can still see clearly that both the TDSE results shown in Figs. 7(a) and 7(b) reveal the stripe-like structure observed in the experimental measurements shown in Fig. 7(c). Furthermore, the radial fan-like structure in the low energy region predicted by the TDSE is also confirmed in the experimental 2DMD, especially for the part of $p_{||} < 0$.

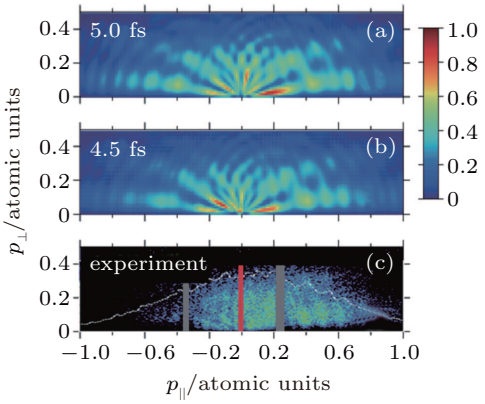


Fig. 7. (color online) Comparison of the TDSE results with the experimental measurements. (a) Volume-integrated TDSE two-dimensional momentum distributions for single ionization of helium by a 5.0-fs laser pulse with a wavelength of 740 nm at the peak intensity of 4.0×10^{14} W/cm^2 with a CEP of $\phi = \pi/2$. (b) Same as panel (a) but for 4.5 fs. (c) The experimental measurements taken from Fig. 4 in Ref. [11] with the ratio of width to height adjusted and the TDSE results removed.

The position of the stripe-like structure predicted by the TDSE with a 4.5-fs pulse in Fig. 7(b) is in better agreement with the experiment than that in Fig. 7(a) with a 5-fs pulse. This can be seen more clearly in Fig. 8 in which the projection of the 2DMD from TDSE onto the $p_{||}$ axis is compared with the experimental distributions. One can see from Fig. 8 that the theoretical results with a 4.5-fs pulse are in overall good agreement with the experimental data, except for the central part around $p_{||} = 0$ where the counts are underestimated by the TDSE. Since the position of the stripe-like structure is very sensitive to the pulse duration, this comparison can be used to determine the pulse duration of the laser pulses used in experiments.

Furthermore, in Fig. 9, we plot the momenta $p_{||}$ where interference peaks occur in Fig. 8. The stripe-like structure in the 2DMD in Fig. 7 corresponds to the peak numbers 5, 6, and 7 in Fig. 9. Again, unsurprisingly, all the positions of the interference peaks are predicted exactly by the TDSE with a 4.5-fs pulse, while with a 5-fs pulse, the TDSE predicts peaks at larger momenta for the peak numbers greater

than 4. It can be seen from Fig. 9 that the spacing between peaks for short pulses is distinctly different from that of regular ATI peaks with a square-root behavior when long laser pulses are used. This has been attributed to the fact that in ultrashort pulses, interferences emerging from wave packet emission at the maxima of the oscillating electric field, i.e., at the carrier frequency corresponding to the photon energy of $\hbar\omega$, are widely suppressed.[11] As a result, quite regular spacing emerges as nearly a linear function of $p_{||}$.

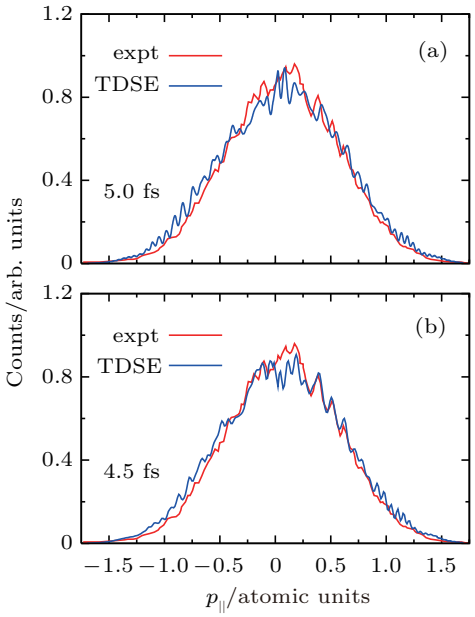


Fig. 8. (color online) Projection of the experimental two-dimensional momentum distributions at a CEP of $\phi = \pi/2$ onto the $p_{||}$ axis taken from Fig. 2(b) in Ref. [11], compared with the volume-integrated TDSE results for single ionization of helium by (a) 5.0-fs and (b) 4.5-fs laser pulses with a wavelength of 740 nm at the peak intensity of 4.0×10^{14} W/cm^2 with a CEP of $\phi = \pi/2$.

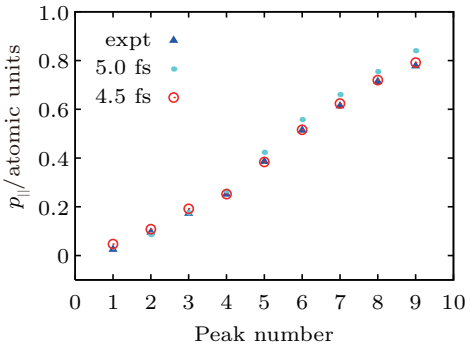


Fig. 9. (color online) Positions of peaks in the parallel momentum $p_{||}$ extracted from Fig. 8.

4. Conclusions

We have investigated recent experimental measurements on the single ionization of helium in few-cycle intense laser pulses[11] by using the SFA model and solving the TDSE. By setting the time window function in the SFA model to control the release time of electrons, we have identified the typical pattern of the intra- and inter-cycle interferences, and found that the vertical stripe-like structure observed in the experimental 2DMD can be attributed to the interplay between the intra- and inter-cycle interferences. It has also been found that the TDSE calculations with the focal-volume effect taken into account are in overall good agreement with the experimental data and the stripe-like structure can be predicted by the TDSE very well. In addition, we have demonstrated that the position of the stripe-like structure can be used to determine the pulse duration of the laser field used in experiments.

References

[1] Rudenko A, Zrost K, Schröter C D, de Jesus V L B, Feuerstein B, Moshammer R and Ullrich J 2004 *J. Phys. B: At. Mol. Opt. Phys.* **37** L407
[2] Maharjan C M, Alnaser A S, Litvinyuk I, Ranitovic P and Cocke C L 2006 *J. Phys. B: At. Mol. Opt. Phys.* **39** 1955
[3] Freeman R R, Bucksbaum P H, Milchberg H, Darack S, Schumacher D and Geusic M E 1987 *Phys. Rev. Lett.* **59** 1092
[4] Chen Zhangjin, Morishita T, Le A T, Wickenhauser M, Tong X M and Lin C D 2006 *Phys. Rev. A* **74** 053405
[5] Paulus G G, Grasbon F, Walther H, Villoresi P, Nisoli M, Stagira S, Priori E and De Silvestri S 2001 *Nature* **414** 182
[6] Paulus G G, Lindner F, Walther H, Baltuška A, Goulielmakis E, Lezius M and Krausz F 2003 *Phys. Rev. Lett.* **91** 253004
[7] Apolonski A, Dombi P, Paulus G G, Kakehata M, Holzwarth R, Udem Th, Lemell Ch, Torizuka K, Burgdörfer J, Hänsch T W and Krausz F 2004 *Phys. Rev. Lett.* **92** 073902
[8] Martiny Christian Per Juul and Madsen Lars Bojer 2006 *Phys. Rev. Lett.* **97** 093001
[9] Wittmann T, Horvath B, Helml W, Schätzel M G, Gu X, Cavalieri A L, Paulus G G and Kienberger R 2009 *Nat. Phys.* **5** 357
[10] Lindner F, Schätzel M G, Walther H, Baltuška A, Goulielmakis E, Krausz F, Milošević D B, Bauer D, Becker W and Paulus G G 2005 *Phys. Rev. Lett.* **95** 040401
[11] Gopal R, Simeonidis K and Moshammer R, *et al.* 2009 *Phys. Rev. Lett.* **103** 053001
[12] Arbó D G, Yoshida S, Persson E, Dimitriou K I and Burgdörfer J 2006 *Phys. Rev. Lett.* **96** 143003
[13] Arbó D G, Ishikawa K L, Schiessl K, Persson E and Burgdörfer J 2010 *Phys. Rev. A* **81** 021403(R)
[14] Arbó D G, Ishikawa K L, Schiessl K, Persson E and Burgdörfer J 2010 *Phys. Rev. A* **82** 043426
[15] Bian X B, Huismans Y and Smirnova O, *et al.* 2011 *Phys. Rev. A* **84** 043420
[16] Arbó D G, Ishikawa K L, Persson E and Burgdörfer J 2012 *Nucl. Instrum. Method Phys. Res. B* **279** 24
[17] Lewenstein M, Balcou P, Ivanov M Y, L'Huillier A and Corkum P B 1994 *Phys. Rev. A* **49** 2117
[18] Chen Zhangjin, Morishita T, Le A T and Lin C D 2007 *Phys. Rev. A* **76** 043402
[19] Tong X M and Lin C D 2005 *J. Phys. B: At. Mol. Opt. Phys.* **38** 2593
[20] Tong X M and Chu S I 1997 *Chem. Phys.* **217** 119
[21] Morishita T, Chen Zhangjin, Watanabe S and Lin C D 2007 *Phys. Rev. A* **75** 023407
[22] Harris D O, Engerholm G G and Gwinn W D 1965 *J. Chem. Phys.* **43** 1515
[23] Dickinson A S and Certain P R 1968 *J. Chem. Phys.* **49** 4209
[24] Light J C and Walker R B 1976 *J. Chem. Phys.* **65** 4272
[25] Remetter T, Johnsson P, Mauritsson J, Varjú K, Ni Y, Lépine F, Gustafsson E, Kling M, Khan J, López-Martens R, Schafer K J, Vrakking M J J and L'uillier A 2006 *Nat. Phys.* **2** 323